

One-dimensional spin texture of Bi(441): Quantum spin Hall properties without a topological insulator

M. Bianchi,¹ F. Song,^{2,3} S. Cooil,^{4,5} Å. F. Monsen,⁵ E. Wahlström,⁵ J. A. Miwa,¹ E. D. L. Rienks,⁶ D. A. Evans,⁴ A. Strozecka,⁷ J. I. Pascual,⁸ M. Leandersson,⁹ T. Balasubramanian,⁹ Ph. Hofmann,¹ and J. W. Wells^{5,*}

¹*Department of Physics and Astronomy, Interdisciplinary Nanoscience Center (iNANO), University of Aarhus, 8000 Aarhus C, Denmark*

²*Zernike Institute of Advanced Materials, University of Groningen, 9747 AG, The Netherlands*

³*Shanghai Institute of Applied Physics, Chinese Academy of Science, 201204, P. R. China*

⁴*Department of Physics, Aberystwyth University, Aberystwyth, UK. SY23 3BZ*

⁵*Department of Physics, Norwegian University of Science and Technology (NTNU), Trondheim, Norway*

⁶*Helmholtz-Zentrum Berlin, Albert-Einstein-Str. 15, 12489 Berlin, Germany*

⁷*Institut für Experimentalphysik, Freie Universität Berlin, Arnimallee 14, 14195 Berlin, Germany*

⁸*CIC nanoGUNE, 20018 Donostia-San Sebastián, Spain*

⁹*MAX IV Laboratory, Lund University, P.O. Box 118, 221 00 Lund, Sweden*

(Received 25 August 2014; revised manuscript received 31 January 2015; published 21 April 2015)

The high index (441) surface of bismuth has been studied using scanning tunneling microscopy (STM), angle resolved photoemission spectroscopy (APRES), and spin-resolved ARPES. The surface is strongly corrugated, exposing a regular array of (110)-like terraces. Two surface localized states are observed, both of which are linearly dispersing in one in-plane direction (k_x), and dispersionless in the orthogonal in-plane direction (k_y), and both of which have a Dirac-like crossing at $k_x = 0$. Spin ARPES reveals a strong in-plane polarization, consistent with Rashba-like spin-orbit coupling. One state has a strong out-of-plane spin component, which matches with the miscut angle, suggesting its possible origin as an edge state. The electronic structure of Bi(441) has significant similarities with topological insulator surface states and is expected to support one-dimensional quantum spin Hall-like coupled spin-charge transport properties with inhibited backscattering, without requiring a topological insulator bulk.

DOI: [10.1103/PhysRevB.91.165307](https://doi.org/10.1103/PhysRevB.91.165307)

PACS number(s): 73.43.-f, 73.20.-r

Bismuth is an interesting material for many reasons [1–4]. Being the heaviest stable element, spin-orbit interactions are especially significant [5], making it an ideal platform for testing fundamental concepts such as spin nondegeneracy limiting impurity scattering [6] and inhibiting a charge density wave [7]. The heavy nuclear weight can also cause a parity inversion such that semiconducting bismuth alloys can support an inverted band gap and the creation of a topological insulator phase [8]. Such topological insulators have attracted much interest [9] and have been suggested as candidates for a range of potential device applications [10,11].

Bismuth and many of its compounds are layered materials. As with graphene, ultrathin bismuth is reported to be a two-dimensional (2D) topological insulator [12–15] supporting an edge-localized quantum spin Hall (QSH)-like state. The vicinal surface of bismuth, Bi(114) [16,17], consists of an array of such edges and supports a single one-dimensional Fermi contour, which has been revealed to be nondegenerate with respect to spin and is reminiscent of a topological insulator state.

Here, we investigate the surface electronic structure and spin texture of another vicinal bismuth surface: Bi(441). A scanning tunneling microscopy (STM) study was performed, and the rhombic surface unit cell of Bi(441) is seen. The (441) surface is observed to support a 2×2 reconstruction which is well described by a simple truncated bulk “missing-row” model [see Figs. 1(a)–1(c)], thus the surface can be viewed as a regular 1D array of (110)-oriented domains, with edges of the (111) bilayers exposed.

Using angle resolved photoemission spectroscopy (ARPES) we show that the surface electronic structure is strongly influenced by the vicinity of the surface. In fact, the Fermi surface consists almost entirely of a single 1D feature which passes through the surface Brillouin zone (SBZ) center, $\bar{\Gamma}$ [see Fig. 1(d)]. As in the case of Bi(114), the Fermi surface shows no sign of the 2×2 surface reconstruction. Whilst the periodicity in k_x is clear, there is a lack of dispersion in k_y . The lack of periodicity in the surface Fermi surface highlights the model 1D behavior of the sample since k_y becomes an irrelevant parameter in the perfect 1D case.

An additional weak and broad feature (visible as a faint “X”) is also present in the ARPES measurement [Fig. 1(d)]. By considering its dispersion with photon energy, it can be attributed to a projected bulk state. This view is strongly supported by tight binding calculations [see Fig. 1(e) and the Supplemental Material [19]]. There is a lack of bulk symmetry in the y direction which hinders a simple identification of $k_y = 0$. However, the tight binding calculated bulk band projection allows $\bar{\Gamma}$ to be identified.

The single 1D feature in the Fermi surface raises the question of the nature of this state. Strong spin-orbit coupling is expected [4], and states reminiscent of topological insulator surface have been observed on other bismuth [16,20,21] (and $\text{Bi}_x\text{Sb}_{1-x}$ [21,22]) surfaces. However, if bulk bismuth is described as topologically trivial [23–25] then an unpaired Fermi level crossing is not expected here.

Since the surface can be viewed as an array of (111) bilayer edges, an alternative approach is to consider the arguments of topology in a similar way; bilayer bismuth (111) is described

*quantum.wells@gmail.com

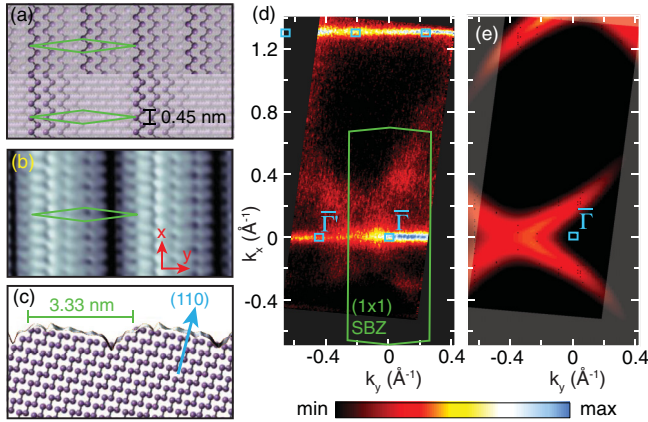


FIG. 1. (Color online) (a) Truncated bulk model of the surface, showing the 1×1 (upper half) and the missing row (lower half) reconstruction. The 1×1 unit cell is superimposed in green. (b) STM image (bias voltage = 0.091 V, tunneling current = 90 pA), similarly scaled with the same unit cell overlaid. (c) Side view of the 2×2 truncated bulk model and the measured STM height profile. (d) Fermi surface map performed with photon energy $h\nu = 70$ eV, showing the 1×1 SBZ and the Γ points. Bright colors (light blue, white, yellow) indicate high intensity and dark colors (black, dark red) indicate low intensity. (e) Tight binding calculated constant energy surface indicating where the projected bulk states are close enough to the measured Fermi surface for a weak intensity contribution to be expected [using the parameters of Liu and Allen (Ref. [18])].

as topologically nontrivial in its 2D bulk, thus its 1D edges can be expected to support a topological state. In a simplified view, the high index surfaces of the form $(x, x, 1)$ behave as an array of such (111) bilayer edges, coupled only by van der Waals forces. The lack of strong interaction between the layers is manifest in the 1D Fermi surface, thus it is perhaps reasonable to expect that the 1D state inherits the characteristics of the bilayer's topological edge state [14,26].

Measurements made at a range of photon energies (Fig. 2) reveal the existence of two Dirac-like states, with very

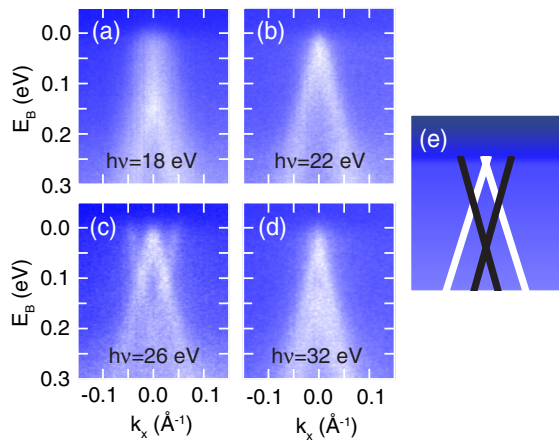


FIG. 2. (Color online) (a)–(d) ARPES measurements performed at $k_y = 0 \text{ \AA}^{-1}$ and photon energies 18, 22, 26, and 32 eV, respectively. (e) Schematic depicting the presence of “inner” (white) and “outer” (black) Dirac-like states.

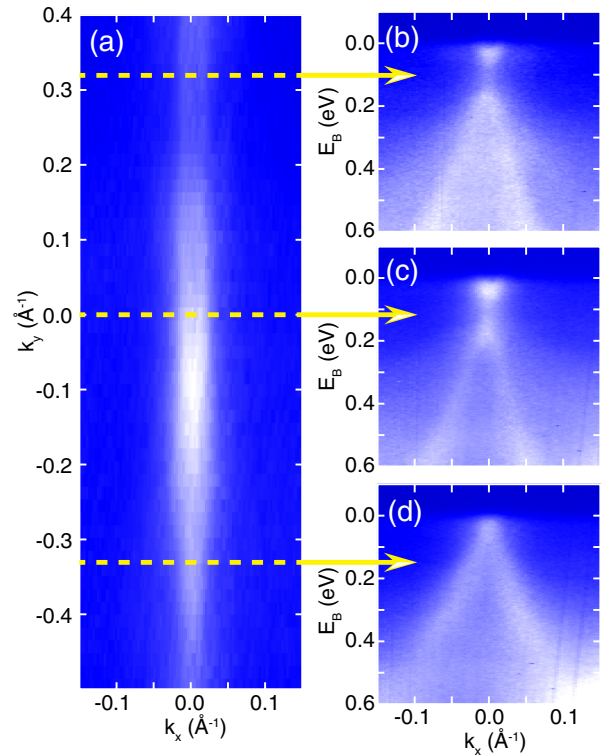


FIG. 3. (Color online) (a) Fermi surface collected with photon energy 19 eV. Yellow horizontal lines indicate where the slices shown in (b), (c), and (d) have been extracted ($k_y = +0.33$, $k_y = 0$, and $k_y = -0.33 \text{ \AA}^{-1}$, respectively).

similar dispersions in the k_x direction. Their cross sections vary strongly, thus typically only one state dominates the measurement. At particular photon energies, both states are visible, for example at $h\nu = 26$ eV [Fig. 2(c)]. A likely cause of this strong variation in intensity is a corresponding variation in the matrix element describing the photo excitation to a bulklike final state [27]. The lack of dispersion with photon energy (or equivalently k_{\perp} [28]) confirms that these states are surface or edge states. Our tight binding calculations of the bulk states (which are otherwise in good agreement with the measurements) do not reproduce these states, further supporting the notion that neither of these states are bulklike.

The photoemission intensity at the Fermi level [Fig. 3(a)], collected at a photon energy of 19 eV, shows that this state has an apparent dependence on k_y . This is best seen in the constant k_y slices taken at $k_y = +0.33$, $k_y = 0$, and $k_y = -0.33 \text{ \AA}^{-1}$, which reveal a pair of linearly dispersing branches [see Figs. 3(b)–3(d)] with Dirac-like crossings at $k_x = 0$ with $E_B \approx 150$, $E_B \approx 150$, and $E_B \approx 0$ meV for $k_y = +0.33$, $k_y = 0$, and $k_y = -0.33 \text{ \AA}^{-1}$, respectively.

Although the binding energy of the Dirac-like crossing is seen to depend on k_y , this is not due to dispersion. Instead the intensity of the state at deeper binding energy [presented schematically in Fig. 2(e), black trace], and the state with the crossing nearest the Fermi level [Fig. 2(e), white trace], depends strongly on k_y . At any particular value of k_y (such as the slices in Fig. 3), the photoemission intensity is dominated by one of the states. In other words, the binding energies of the

two Dirac-like crossing points do not depend on k_y , however, there is an apparent dependence on binding energy due to the strong change in the relative intensity of the two states.¹ Thus, both states have a true 1D nature.

Since strong spin-orbit coupling is expected in this material [4,7,16,29], we probe the spin polarization of the states observed here by Spin-ARPES, using a Mott-type detector [30]. The small k_x separation of the observed states requires good experimental resolutions, with measurements at low photon energy being preferable. For example, at photon energy 9 eV, the spin polarization can be efficiently measured: The state with its crossing point closest to the Fermi level [marked in white in Fig 2(e)] is most intense, and hence dominates the ARPES measurement, although a very weak remnant of the outermost state is barely visible [see Fig. 4(a)]. Correspondingly, this state dominates the spin-ARPES measurement, and hence its polarization can be found unambiguously. The spin-ARPES measurements were performed as two momentum distribution curves (MDCs), one at the Fermi level and the other around 200 meV below. A 2D Mott detector is oriented such that the out-of-plane spin component and the in-plane component in the y direction are measured. The raw spin-polarization P is given by $P = \chi(N_+ - N_-)/(N_+ + N_-)$, where N_+ and N_- are the number of counts recorded by the detectors in the relevant positive and negative directions (i.e., “up” and “down” for the in-plane polarization and “left” and “right” for the out-of-plane polarization). Since the four detectors are not equally sensitive, a sensitivity factor χ is found by evaluating $\chi = (N_+ + N_-)/(N_+ - N_-)$ well above the Fermi level. In other words, the polarization of the state is evaluated relative to a background measurement. It should be noted that no other corrections are made; no Sherman function is assumed, hence “raw” polarization is stated.

At photon energy 9 eV [Fig. 4(a)], two MDCs are selected to cross the state above and below its degenerate crossing at $k_x = 0$. In both spin MDCs, the maximum polarization is seen at $k_x \approx \pm 0.02 \text{ \AA}^{-1}$ [Figs. 4(b) and 4(c)], corresponding to the maximum intensity of the state. In both cases, the out-of-plane component (gray) shows no significant polarization, whereas the in-plane component (blue-red) shows a strong sign reversal: negative to positive near the Fermi level and positive to negative at $E_b \approx 0.2 \text{ eV}$, typical of a Rashba-like coupling. The raw spin polarization is between 6 and 8%, which, after allowing for a nonpolarized background, and correcting for the Sherman function ($\approx 17\%$) indicates that the state is very strongly polarized.

In order to observe the spin polarization of the second state [with its crossing point at around $E_B = 200 \text{ meV}$ and schematically depicted in black in Fig. 2(e)], the observed strong intensity variation with photon energy is exploited. At $h\nu = 26 \text{ eV}$, this state appears more intense, however both states are contributing some intensity to the signal. Once again spin MDCs can be performed at the Fermi level and

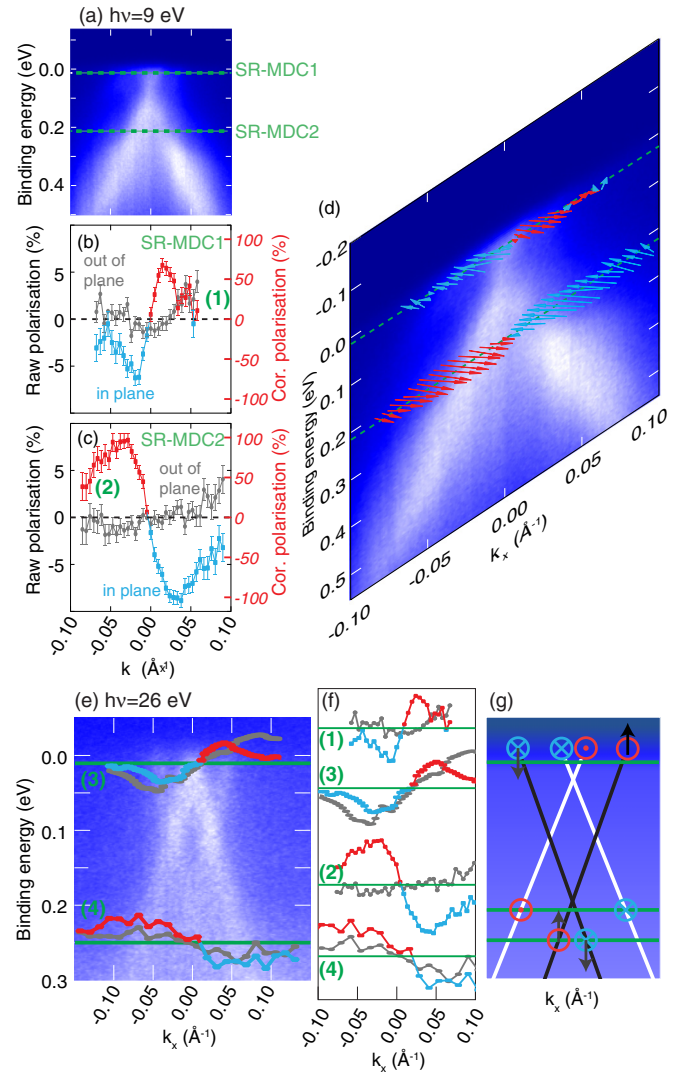


FIG. 4. (Color online) (a) ARPES measurement performed at $h\nu = 9 \text{ eV}$ showing where two spin resolved MDCs (SR-MDC1 and SR-MDC2) were collected (green dashed lines). (b) and (c) The raw spin polarizations collected at the Fermi level and at $E_b = 0.2 \text{ eV}$, respectively, showing the in-plane (blue-red) and out-of-plane (gray) spin components. The red axis indicates *corrected polarization*, found by subtracting a nonpolarized background and correcting for the Sherman function of 17%. (d) ARPES measurement with the reconstructed spin vectors superposed. (e) In-plane (blue-red) and out-of-plane (gray) spin components from SR-MDCs atop an ARPES measurement at $h\nu = 26 \text{ eV}$, where the contribution of the outer state is stronger. In both cases $k_y = 0$. (f) Similarly scaled polarization curves for the four SR-MDCs numbered in (a)–(c) and (e). (g) Schematic representation of the measured spin vectors and the positions at which they are measured.

at higher binding energy ($\approx 0.25 \text{ eV}$). The maximum observed polarization at the Fermi level is now seen at $k_x \approx 0.05 \text{ \AA}^{-1}$, corresponding to the maximum intensity of the outer state [Fig. 4(e)]. As before, a strong reversal in the in-plane polarization (from negative to positive at the Fermi level) is seen, indicating that the in-plane polarization of both states is the same. Contrary to the previous case, the out-of-plane

¹A close inspection of many constant k_y slices reveals that there is a very weak dispersion in k_y ; the positions of the Dirac points vary by $\approx 30 \text{ meV}$.

component is now of a similar magnitude to the in-plane component, indicating that the spin vector is approximately 45° to the sample surface. The MDC at larger binding energy shows a weaker polarization reversal, probably because both surface states, and perhaps the nearby bulk state are contributing to the intensity. However, this MDC shows a clear reversal of both the in-plane and out-of-plane components, from positive (at negative k_x) to negative (at positive k_x).

The results from the spin MDCs are summarized in Fig. 4(f). The measured polarizations are superposed on the ARPES data for the two relevant photon energies [Figs. 4(d) and 4(e)]. A schematic summary [Fig. 4(g)] sketches the in-plane and out-of-plane components and indicates which band the spin measurements are sensitive to. At the Fermi level, all states have a simple Rashba-like in-plane component, whereas the outer branches also have a large out-of-plane component.

The picture of the electronic structure presented here is broadly consistent with other 1D systems in which SOC is important [31,32]. For example, previous studies of 1D metallic structures on high index silicon surfaces show Rashba-like coupling and a 1D Fermi contour [31]. However, these metallic structures on high index silicon surfaces also show a coupling of the 1D states which is not seen for Bi(441), despite the separation of the 1D chains being significantly less in the present case [33]. In our case of Bi(441), the Fermi contour shows ideal noncoupled 1D behavior.

In the present case of Bi(441), the observed surface states have a dispersion which is more akin to topological insulator surface states than the Rashba coupled free-electron-like parabola of decorated vicinal silicon [31,32]. Since alloying bismuth, for example forming $\text{Bi}_{1-x}\text{Sb}_x$, can result in the formation of a topological insulator phase [34], it is reasonable to assume that $\text{Bi}_{1-x}\text{Sb}_x(441)$ could support an odd number of nontrivial states derived from the states observed here.

The implications of this surface electronic structure for the charge/spin transport properties are important. The spin texture of the band structure is such that a reversal of k_x requires an accompanying spin reversal, i.e., $\epsilon(k_x, \uparrow) \Rightarrow \epsilon(-k_x, \downarrow)$. This means that unless there is a mechanism for exchanging spin angular momentum with an impurity, the probability of a charge carrier (with $E \approx E_F$ and $k_x \approx k_{x,F}$) being backscattered by an impurity approaches zero. Furthermore, there are no other surface states at the Fermi level which allow scattering process which conserve $|\mathbf{k}|$ and E , thus the probability of momentum conserving scattering events is expected to be vanishing small. Indeed, in our STM investigations, there are no visible indications of scattering around impurities. The lack of defect scattering, the spin texture, and the 1D Fermi contour suggest that Bi(441) should have transport properties akin to quantum spin Hall (QSH) materials [35], which are desirable for emergent spintronic applications [9,36].

Although the surface properties of Bi(441) show much promise for spintronics, there is a sufficient contribution of unpolarized bulk states to dominate the transport [37]. In order to utilize the surface spin-transport properties in a real device, it would be necessary to reduce the contribution from the bulk. Two possible methods to achieve this are bulk alloying (for example with Sb, to open a bulk band gap [38]) and by growth of a vicinal thin layer on a semiconducting substrate such as silicon [39,40].

The existence of a finite out-of-plane spin component is also intriguing. In the simple topological insulator case, or indeed for simple Rashba-like SOC, the spin vector at the Fermi level is perpendicular to both the surface and the momentum vector, yielding an entirely in-plane spin vector. For the high index surface Bi(114), a significant out-of-plane component (30°) has been reported [16], which is comparable to the present case of around 45° for Bi(441). In both cases, this coincides with the miscut from the (111) plane. In other words, although superficially similar to the decorated vicinal silicon case [31,32], the two states observed here are not simply SOC branches of the same state but rather have quite separate origins; it is tempting to speculate that the state with a strong out-of-plane component originates from a topological-like edge state of a (111) layer, and the state lacking an out-of-plane component to be the (441) surface state.²

In conclusion, we have presented the electronic structure of a high index surface of bismuth, with a strong 1D surface corrugation. Two 1D states are observed, both of which are nondegenerate with respect to their spin. Bulk bismuth may not be a topological insulator, but is nonetheless close to a topological-insulator transition, thus the states observed can be rationalized as topological-insulator-like, linearly dispersing, spin-polarized states and are expected to support QSH-like coupled spin-charge transport, desirable in emergent spintronic applications.

We thank N. A. Vinogradov and A. B. Preobrajenski for facilitating the motorization of the SR-MDCs, and for helpful discussions. S.C. acknowledges funding from MAX-IV laboratories and Ph.H. acknowledges the VILLUM fonden for financial support.

APPENDIX: METHODS

Samples were prepared by mechanically cutting and polishing a bulk single crystal 45° from the (111) natural cleavage plane. Following mechanical polishing, the orientation was confirmed by Laue diffraction. The sample was then electropolished, introduced into the ultrahigh vacuum chamber and cleaned by multiple cycles of Ar^+ sputtering and very gentle annealing until contaminants were beneath the detection threshold.

ARPES measurements were performed at beamline SGM3 of the synchrotron “ASTRID” in Aarhus, Denmark [41]. Low photon energy ARPES and Spin-ARPES measurements were performed at beamline I3 of MAX-III [30]. STM measurements were performed at Freie Universität Berlin using a custom-made instrument working in ultrahigh vacuum and at low temperature (5 K). Tight binding calculations were performed using the parameters of Liu and Allen [18].

Spin-ARPES were measured using linear-vertical polarized light which was incident upon the sample at 75° from the surface normal. In other words, the polarization vector of the

²As with the Bi(111) edge state, the dispersion is approximately linear around the BZ center, and the crossing point at $k_x = 0$ is close to the Fermi level. However, the band dispersion dE/dk_x observed here is significantly steeper (Ref. [14]).

light is predominantly out-of-plane relative to the sample and with a small component in the k_y direction. Measurements were also made using the same sample geometry and linear-

horizontal light (i.e., in the in-plane k_x direction) and the measured electron spin was the same within the uncertainty of the experiment.

-
- [1] V. S. Édel'man, *Phys. Lett. A* **210**, 105 (1996).
- [2] F. Y. Yang, K. Liu, K. Hong, D. H. Reich, P. C. Searson, and C. L. Chien, *Science* **284**, 1335 (1999).
- [3] E. I. Rogacheva, S. N. Grigorov, O. N. Nashchekina, S. Lyubchenko, and M. S. Dresselhaus, *Appl. Phys. Lett.* **82**, 2628 (2003).
- [4] P. Hofmann, *Prog. Surf. Sci.* **81**, 191 (2006).
- [5] X. Gonze, J. P. Michenaud, and J. P. Vignerot, *Physica Scripta* **37**, 785 (1988).
- [6] A. Strozecka, A. Eiguren, and J. I. Pascual, *Phys. Rev. Lett.* **107**, 186805 (2011).
- [7] T. K. Kim, J. Wells, C. Kirkegaard, Z. Li, S. V. Hoffmann, J. E. Gayone, I. Fernandez-Torrente, P. Häberle, J. I. Pascual, K. T. Moore, A. J. Schwartz, H. He, J. C. H. Spence, K. H. Downing, S. Lazar, F. D. Tichelaar, S. V. Borisenko, M. Knupfer, and Ph. Hofmann, *Phys. Rev. B* **72**, 085440 (2005).
- [8] H. Zhang, C.-X. Liu, X.-L. Qi, X. Dai, Z. Fang, and S.-C. Zhang, *Nat. Phys.* **5**, 438 (2009).
- [9] J. E. Moore, *Nature (London)* **464**, 194 (2010).
- [10] J. J. Cha, J. R. Williams, D. S. Kong, S. Meister, H. L. Peng, A. J. Bestwick, P. Gallagher, D. Goldhaber-Gordon, and Y. Cui, *Nano. Lett.* **10**, 1076 (2010).
- [11] F. Xiu, L. He, Y. Wang, L. Cheng, L.-T. Chang, M. Lang, G. Huang, X. Kou, Y. Zhou, X. Jiang, Z. Chen, J. Zou, A. Shailos, and K. L. Wang, *Nat. Nano.* **6**, 216 (2011).
- [12] Z. Qiao, W.-K. Tse, H. Jiang, Y. Yao, and Q. Niu, *Phys. Rev. Lett.* **107**, 256801 (2011).
- [13] M. Wada, S. Murakami, F. Freimuth, and G. Bihlmayer, *Phys. Rev. B* **83**, 121310 (2011).
- [14] S. Murakami, *Phys. Rev. Lett.* **97**, 236805 (2006).
- [15] L. Chen, Z. F. Wang, and F. Liu, *Phys. Rev. B* **87**, 235420 (2013).
- [16] J. W. Wells, J. H. Dil, F. Meier, J. Lobo-Checa, V. N. Petrov, J. Osterwalder, M. M. Ugeda, I. Fernandez-Torrente, J. I. Pascual, E. D. L. Rienks, M. F. Jensen, and Ph. Hofmann, *Phys. Rev. Lett.* **102**, 096802 (2009).
- [17] D. Leuenberger, H. Yanagisawa, S. Roth, J. H. Dil, J. W. Wells, P. Hofmann, J. Osterwalder, and M. Hengsberger, *Phys. Rev. Lett.* **110**, 136806 (2013).
- [18] Y. Liu and R. E. Allen, *Phys. Rev. B* **52**, 1566 (1995).
- [19] See Supplemental Material at <http://link.aps.org/supplemental/10.1103/PhysRevB.91.165307> for details of the tight binding calculations.
- [20] C. R. Ast and H. Höchst, *Phys. Rev. Lett.* **87**, 177602 (2001).
- [21] S. Agergaard, C. Søndergaard, H. Li, M. B. Nielsen, S. V. Hoffmann, Z. Li, and P. Hofmann, *New J. Phys.* **3**, 15 (2001).
- [22] X.-G. Zhu, M. Stensgaard, L. Barreto, W. S. e Silva, S. Ulstrup, M. Michiardi, M. Bianchi, M. Dendzik, and P. Hofmann, *New J. Phys.* **15**, 103011 (2013).
- [23] P. Hofmann, J. E. Gayone, G. Bihlmayer, Y. M. Koroteev, and E. V. Chulkov, *Phys. Rev. B* **71**, 195413 (2005).
- [24] J. C. Y. Teo, L. Fu, and C. L. Kane, *Phys. Rev. B* **78**, 045426 (2008).
- [25] Y. Ohtsubo, L. Perfetti, M. O. Goerbig, P. L. Fèvre, F. Bertran, and A. Taleb-Ibrahimi, *New J. Phys.* **15**, 033041 (2013).
- [26] I. K. Drozdov, A. Alexandradinata, S. Jeon, S. Nadj-Perge, H. Ji, R. J. Cava, B. A. Bernevig, and A. Yazdani, *Nature Physics* **10**, 664 (2014).
- [27] J. A. Miwa, P. Hofmann, M. Y. Simmons, and J. W. Wells, *Phys. Rev. Lett.* **110**, 136801 (2013).
- [28] F. J. Himpsel, *Appl. Opt.* **19**, 3964 (1980).
- [29] Y. M. Koroteev, G. Bihlmayer, J. E. Gayone, E. V. Chulkov, S. Blügel, P. M. Echenique, and P. Hofmann, *Phys. Rev. Lett.* **93**, 046403 (2004).
- [30] M. H. Berntsen, P. Palmgren, M. Leandersson, A. Hahlin, J. Ahlund, B. Wannberg, M. Mansson, and O. Tjernberg, *Rev. Sci. Instrum.* **81**, 035104 (2010).
- [31] I. Barke, F. Zheng, T. K. Rügheimer, and F. J. Himpsel, *Phys. Rev. Lett.* **97**, 226405 (2006).
- [32] C. Tegenkamp, D. Lükermann, H. Pfnür, B. Slomski, G. Landolt, and J. H. Dil, *Phys. Rev. Lett.* **109**, 266401 (2012).
- [33] I. Barke, T. K. Rügheimer, F. Zheng, and F. J. Himpsel, *Appl. Surf. Sci.* **254**, 4 (2007).
- [34] X.-G. Zhu and P. Hofmann, *Phys. Rev. B* **89**, 125402 (2014).
- [35] B. A. Bernevig and S.-C. Zhang, *Phys. Rev. Lett.* **96**, 106802 (2006).
- [36] D. Pesin and A. H. MacDonald, *Nat. Mater.* **11**, 409 (2012).
- [37] J. W. Wells, K. Handrup, J. F. Kallehauge, P. Bøggild, M. B. Balslev, J. E. Hansen, P. R. E. Petersen, and P. Hofmann, *J. Appl. Phys.* **104**, 053717 (2008).
- [38] F. Nakamura, Y. Kousa, A. A. Taskin, Y. Takeichi, A. Nishide, A. Kakizaki, M. D'Angelo, P. Lefevre, F. Bertran, A. Taleb-Ibrahimi, F. Komori, S.-i. Kimura, H. Kondo, Y. Ando, and I. Matsuda, *Phys. Rev. B* **84**, 235308 (2011).
- [39] J. W. Wells, J. F. Kallehauge, and P. Hofmann, *J. Phys. Condens. Matter* **19**, 176008 (2007).
- [40] W. Ning, F. Kong, Y. Han, H. Du, J. Yang, M. Tian, and Y. Zhang, *Sci. Rep.* **4**, 7086 (2014).
- [41] S. V. Hoffmann, C. Søndergaard, C. Schultz, Z. Li, and P. Hofmann, *Nucl. Instrum. Methods Phys. Res., Sect. A* **523**, 441 (2004).